Progress In Electromagnetics Research Letters, Vol. 30, 125–132, 2012

RADIAL LOADED TRANSFORMED RADIAL STUB FOR LPF STOPBAND EXTENSION

K. Ma*, S. X. Mou, K. P. Wang, and K. S. Yeo

School of Electrical and Electronic Engineering, Nanyang Technological University, Singapore

Abstract—A low pass filter with ultra-wide band rejection and compact size using a proposed radial loaded transformed radial stubs is introduced and investigated. The implemented unite cell low pass filter with 1-dB cutoff frequency f_c of 3.2 GHz demonstrates stopband rejection up to 11.8 f_c, i.e., 38 GHz. The design is further extended to the high-order LPF through cell cascading. The implemented four-cell LPF with f_c of 3.6 GHz demonstrated 35 dB rejection from 4.8 GHz to 39 GHz, 50 dB rejection from 5.4 GHz to 26 GHz (7.2 f_c) and 20 dB rejection from 4.4 GHz to 50 GHz (13.8 f_c). The measured passband insertion loss is less than 1.7 dB, and group delay is $0.45 \sim 0.8$ nS. The size of the four-cell low pass filter is only $0.33\lambda_g \times 0.135\lambda_g$, ($\lambda_g$ is the guide wavelength at center cutoff frequency) without using any lumped elements.

1. INTRODUCTION

Low-pass filters (LPFs) are a crucial type of filters in the filter family. It is adopted to remove undesired harmonics or spurious of the nonlinear circuits in RF front-end. Wide stopband and high stopband rejection are important for LPF to improve the linearity and signal over noise ratio especially in the high data rate and wideband communication systems [1–12]. A good LPF is needed to suppress the mixed frequency elements and leakages of radio frequency (RF) and local oscillator (LO) frequency from the mixer. The merits of stepped-impedance hairpin resonators are their relatively smaller size and additional zeros in the stopband achieved through additional electric coupling path

Received 20 January 2012, Accepted 24 February 2012, Scheduled 5 March 2012

* Corresponding author: Kaixue Ma (kxma@ntu.edu.sg).

[1–3]. Recently, defected ground structure (DGS) usage in the LPFs for wide stopband has been demonstrated [4–6]. A new low pass configuration using transformed radial stubs (TRS), formed by the coupled line transformer connected with a radial stub (the radial stub has intrinsic wide stopband characteristics [7, 8]), is proposed in [9, 10]. The implemented LPF with a planar configuration and free of lumped resistor-inductor-capacitor (R-L-C) elements demonstrates an ultra-wide stopband stopband rejection better than 25 dB up to 24 GHz (8 f_c). However, the stopband is only up to 24 GHz i.e., 8 f_c, which may not be enough for some applications such as millimeter-wave communication or radar. In this paper, while keeping the same size as the TRS LPF, we further extend the stopband of the TRS LPF cell up to 13.8 f_c by introducing the radial loading at the transformer ends, which almost do not change the overall size of the TRS LPF. Meanwhile, a equivalent circuit model is introduced for the investigation of the proposed LPF. A low pass configuration as shown in Figs. 1(c) and (d) using radial loaded transformed radial stubs (RLTRS) as shown in Fig. 1, which is formed by the coupled line transformer connected with one big radial stub in one end and two smaller radial stubs in the other end, is proposed and investigated to achieve a unique planar non-lumped-element LPF with steep rolloff, ultra wide stopband, compact size and low cost simultaneously. The implemented four-cell LPF with f_c of 3.6 GHz demonstrated 35 dB rejection from 4.8 GHz to 39 GHz, i.e., 10.8 f_c, 50 dB rejection from 5.4 GHz to 26 GHz (7.2 f_c)and 20 dB rejection from 4.4 GHz to 50 GHz (13.8 f_c) and the size only of $0.33\lambda_g \times 0.135\lambda_g$. To the best of the authors' knowledge, it is the best performance of the planar non-lumped element LPFs reported in the publication.

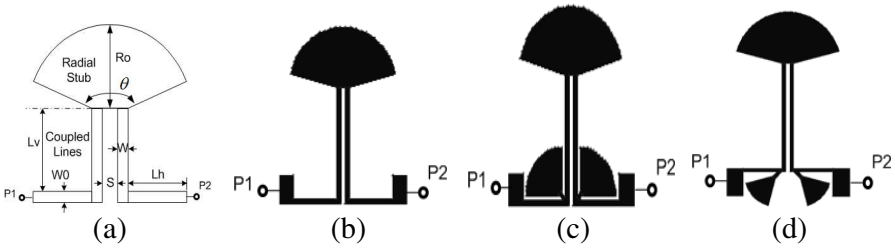

Figure 1. Proposed different type of the TRS LPF cells. (a) TRS LPF cell. (b) Layout of TRS LPF. (d) Loaded TRS LPF. (d) Radial loaded TRS LPF.

2. LOADED TRS LPF CELLS

Figures 1(c) and (d) show two types of RLTRS LPF cell. Both of the structures could be approximately equivalent to the circuit elements as shown in Fig. 2(a). The circuit in Fig. 1(a) can be modeled as the lumped element model as shown in Fig. 2(b). The model of the unit cell can be derived from the transmission line elements, such as radial stubs, coupled lines, and the transmission lines, all of which can be represented as the lumped circuit elements in certain frequency range [10].

For the radial stubs shown in the inset of Fig. 2(a), March [7] obtained the input impedance in the following form:

$$Z_{in} = -\frac{j120\pi h}{r_i\theta\sqrt{\varepsilon_{eff}}}\frac{Y_0(\beta r_i)J_1(\beta r_0) - J_0(\beta r_i)Y_1(\beta r_0)}{J_1(\beta r_i)Y_1(\beta r_0) - Y_1(\beta r_i)J_1(\beta r_0)} \tag{1}$$

where J_x and Y_x are the x-order Bessel functions of the first and second types, respectively, $\beta = 2\pi\sqrt{\varepsilon_{eff}}/\lambda_0$ the phase constant, h is the thickness of the dielectric layer, and ε_{eff} the effective dielectric constant of a microstrip line having a width $W_{eqstub} = (r_0 + r_i)\sin(\theta/2)$. Assuming $r_0 < \lambda_0/8$ and $r_i \approx \lambda_0/10$, we expand the Bessel functions in Equation (1) into a series and keep up to the first order terms, resulting

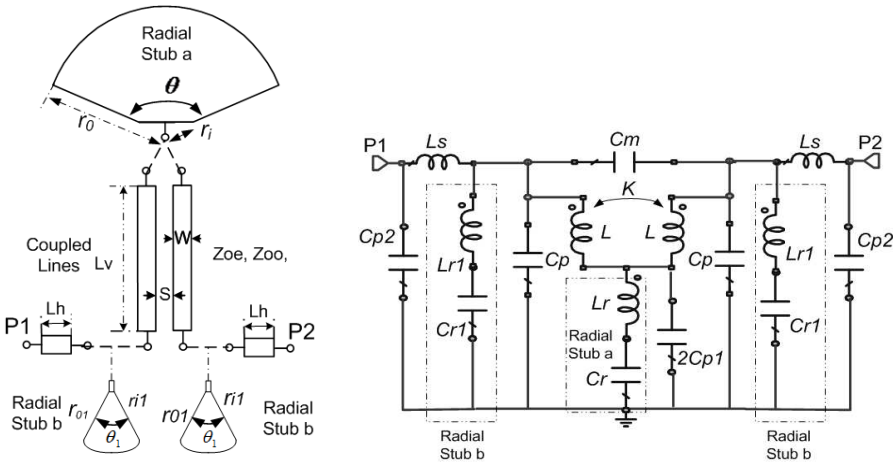

Figure 2. Connections of loaded LPF cell and its equivalent circuit model in Fig. 1(d). (a) Proposed unit LPF cell. (b) Equivalent circuit model of LPF cell.

in

$$Z_{in} \cong -\frac{j120\pi h}{r_i\theta\sqrt{\varepsilon_{eff}}}\left(\frac{2}{\beta r_0^2}-\beta\left(2.8-\frac{10r_i}{r_0}\right)\right) \tag{2}$$

which is equivalent to a series combination of a capacitor C_r and an inductor L_r.

$$C_r \equiv \theta r_0^2\varepsilon_{eff}/(2\pi hc) \tag{3}$$

$$L_r \equiv 120\pi h(2.8-10r_i/r_0)/(c\theta) \tag{4}$$

Here, c is the speed of light. The values for L, K and C_p, etc. can be calculated using Equations (5)–(11) given in [10]:

$$L = \frac{(Z_{oe}+Z_{oo})\sin(\beta L_v)}{4\pi f} \tag{5}$$

$$C_{p1} = \frac{\tan(\beta L_v/2)}{2\pi f Z_{oe}} \tag{6}$$

$$C_m = \left(\frac{1}{Z_{oo}}-\frac{1}{Z_{oe}}\right)\frac{\tan(\beta L_v/2)}{4\pi f} \tag{7}$$

$$k = \frac{Z_{oe}-Z_{oo}}{Z_{oe}+Z_{oo}} \tag{8}$$

$$C_{p2} = \frac{1-\cos(2\beta L_h)}{2\pi f Z_h\cos(2\beta L_h)} \tag{9}$$

$$L_s = \frac{Z_h\sin(\beta L_h)}{2\pi f} \tag{10}$$

$$C_p = C_{p1}+C_{p2} \tag{11}$$

where $Lm = k \times L$. With the transmission line models, the structure in Fig. 1(c) and Fig. 1(d) can be treated as the cascading of the

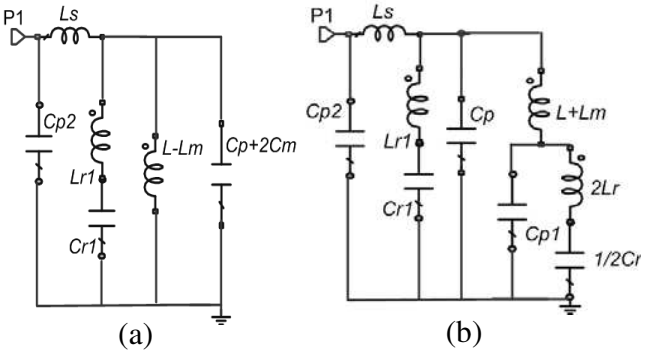

Figure 3. The odd- and even-mode equivalent circuit of the model in Fig. 2. (a) Odd mode. (b) Even mode.

elements as shown in Fig. 2(a). The major element values are given in Equations (3)–(11).

The symmetrical physical based model as shown in Fig. 2(b) can be analyzed using the even- and odd- mode method. The even- and odd- mode equivalent circuits of the derived physical circuit model in Fig. 2(b) are given in Fig. 3(a) and Fig. 3(b), respectively. The even- and odd- mode admittances of the equivalent circuit models can be calculated by using Equations (12) and (13):

$$Y_{ine} = sC_{p2} + \cfrac{1}{sL_s + \cfrac{1}{sC_p + \cfrac{1}{sL_{r1} + \cfrac{1}{sC_{r1}}} + \cfrac{1}{s(L+L_m) + \cfrac{1}{sC_{p1} + \cfrac{1}{s2L_r + \cfrac{2}{sC_r}}}}}} \tag{12}$$

$$Y_{ino} = sC_{p2} + \cfrac{1}{sL_s + \cfrac{1}{s(C_p + 2C_m) + \cfrac{1}{s(L - L_m)} + \cfrac{1}{sL_{r1} + \cfrac{1}{s2C_{r1}}}}} \tag{13}$$

The transmission and reflection response of the proposed equivalent circuits can be calculated through the odd- and even- mode admittances as in [10].

$$S_{21} = \frac{Y_0 Y_{ino} - Y_0 Y_{ine}}{(Y_0 + Y_{ine})(Y_0 + Y_{ino})} \tag{14}$$

$$S_{11} = \frac{Y_0^2 - Y_{ine} Y_{ino}}{(Y_0 + Y_{ine})(Y_0 + Y_{ino})} \tag{15}$$

The RF board RO5880 with dielectric constant of 2.2 and thickness of 10 mil from Rogers Corporation is used in the following design and investigation. The low pass filter is designed with 1 dB cutoff frequency at 3.2 GHz, the stopband to 11.8 f_c and the dimensions of $S = 4$ mil, $L_h = 65$ mil, $L_v = 162$ mil, $\theta = 150$ degrees, $\theta_1 = 60$ degrees, $R_0 = 85$ mil, $R_i = 18$ mil, $R_{01} = 46$ mil, $R_{i1} = 6$ mil, $W = 6$ mil. The simulated and measured results are compared in Fig. 3. The measured specifications of the LPF are: operating frequency of DC $\sim$ 3.2 GHz, insertion loss of smaller than 1.0 dB, stop band rejection in the ranges of 6.42 GHz $\sim$ 38 GHz more than 20 dB, four zero points (ZPs) in stop-band with attenuation over 34 dB (40 dB at 7.46 GHz, 34.2 dB at

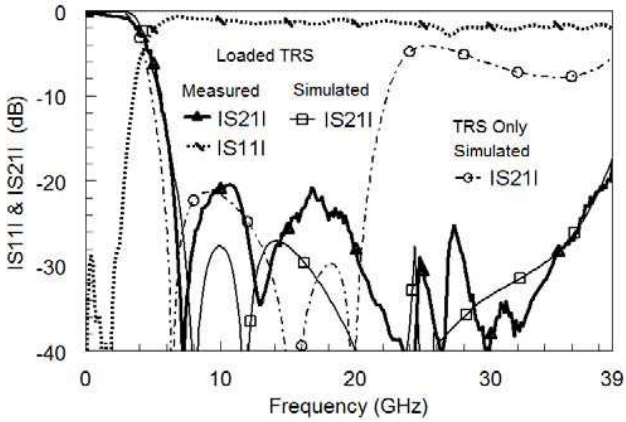

Figure 4. Transmission and reflection characteristics of the unit cell in Fig. 1(d).

12.95 GHz, 40 dB at 24 GHz and 40 dB at 26.4 GHz). Return loss in pass band is less than −20 dB. The results are also compared with the TRS LPF cell as the results shown in Fig. 4. It can be seen that the loaded radial stubs introduce additional two transmission zeros. Thus the stopband of the RLTRS is further extended from 20 GHz up to 39 GHz. Dramatic improvement in the stopband rejection can be seen from 20 GHz to 39 GHz. The RLTRS LPF is very compact with effective size of only 310 mil × 170 mil, i.e., $0.12\lambda_g \times 0.063\lambda_g$.

3. HIGH ORDER RADIAL LOADED TRS LPF DESIGN

Although the unit RLTRS cell has intrinsic excellent stopband with multiple zeros generated in stopband, the stopband rejection as well as the rolloff may not meet some application requirements. The higher order RLTRS LPF by cascading multiple RLTRS cells is designed to further improve the rejection depth and the skirt selectivity. The four-cell RLTRS LPF topology based on cell network cascading in [8] is shown in Fig. 5(a). The implemented filter photograph is shown in Fig. 5(b). The dimensions of the cell are: $S = 4$ mil, $L_h = 65$ mil, $L_v = 168$ mil, $\theta = 150$ degrees, $\theta_1 = 60$ degrees, $R_0 = 85$ mil, $R_i = 18$ mil, $R_{01} = 46$ mil, $R_{i1} = 6$ mil, $W = 6$ mil, Cell connection: $W_c = 18$ mil, $L_c = 45$ mil. The simulated and measured results of the 4-cell RLTRS LPF are compared in Fig. 6. Both results agree well in passband and stopband. The filter has the cutoff frequency of 3.6 GHz, passband return loss greater than 12 dB and stopband rejection better than 35 dB up to 39 GHz (10.8 f_c). From 5.4 GHz to 26 GHz (7.2 f_c),

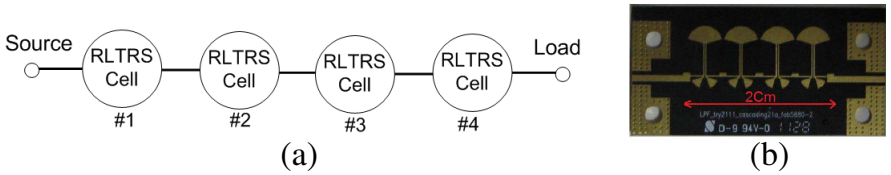

Figure 5. The topology and the photograph of the proposed 4-cell RLTRS LPF. (a) Equivalent Topology. (b) Photograph of the 4-cell RLTRS LPF.

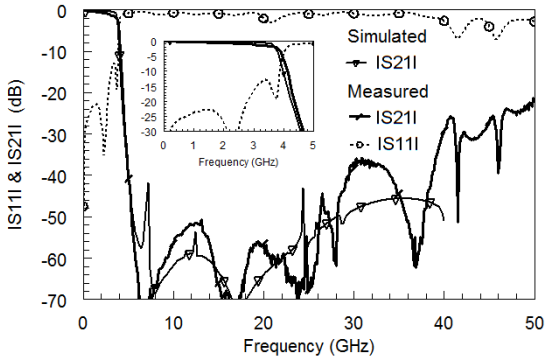

Figure 6. Comparison of the simulation and measurement of the 4-cell RLTRS LPF in Fig. 5.

the rejection is better than 50 dB. The skirt selectivity for the four-cell LPF is up to −122 dB per octave. The measured group delay in the passband is 0.45 ∼ 0.8 ns. The insertion loss is better than 1 dB in DC ∼ 2.8 GHz and better than 1.7 dB from DC to 3.6 GHz. The board sizes of the proposed planar low pass filter, as photograph shown in Fig. 5, is only 20 mm times 8.2 mm ($0.33\lambda_g \times 0.135\lambda_g$).

4. CONCLUSION

In this paper, a radial loaded TRS LPF is proposed and investigated. The physical based equivalent circuit model is derived. The unit cell and four-cell LPFs are designed and implemented to demonstrate the stopband improvement by using radial loading. The measured results of the proposed filters demonstrate not only an ultra-wide stopband, deep stopband rejection, low insertion loss and compact size, but also good group delay and skirt selectivity.

REFERENCES

1. Tu, W.-H. and K. Chang, "Compact microstrip low-pass filter with sharp rejection," *IEEE Microw.. Wireless Compon. Lett.*, Vol. 15, No. 6, 404–406, Jun. 2005.
2. Luo, S., L. Zhu, and S. Sun, "Stopband-expanded low-pass filters using microstrip coupled-line hairpin units," *IEEE Microw. Wireless Compon. Lett.*, Vol. 18, No. 8, 506–508, Aug. 2008.
3. Sheen, J.-W., "A compact semi-lumped low-pass filter for harmonics and spurious suppression," *IEEE Microw. Wireless Compon. Lett.*, Vol. 10, No. 3, 92–93, Mar. 2000.
4. Yang, G. M., R. Jin, J. Geng, X. Huang, and G. Xiao, "Ultra-wideband bandpass filter with hybrid quasi-lumped elements and defected ground structure," *IET Microw.. Antennas Propag.*, Vol. 1, No. 3, 733–736, Jun. 2007.
5. Chen, J., Z.-B. Weng, Y.-C. Jiao, and F.-S. Zhang, "A multi-band meandered slotted-groundplane resonator and its application of low-pass filter," *Progress In Electromagnetics Research*, Vol. 70, 269–280, 2007.
6. Wang, C.-J. and T. H. Lin, "Lowpass filter design of Hilbert curve ring defected ground structure," *Progress In Electromagnetics Research*, Vol. 120, 249–262, 2011.
7. March, S. L., "Analyzing lossy radial-line stubs," *IEEE Trans. Microw. Theory Tech.*, Vol. 33, No. 3, 269–271, Mar. 1985.
8. Ma, K., K. S. Yeo, and Q. Sun, "A novel planar multimode bandpass filter with Radial perturbation," *Microwave and Optical Technology Letters*, Vol. 51, No. 4, 964–966, Apr. 2009.
9. Ma, K. and K. S. Yeo, "Novel low cost compact size planar low pass filters with deep skirt selectivity and wide stopband rejection," *IEEE MTT-S Int. Microwave Symp. Dig.*, 233–236, 2010.
10. Ma, K. and K. S. Yeo, "New ultra-wide stopband low-pass filter using transformed radial stubs," *IEEE Trans. Microw. Theory Tech.*, Vol. 59, No. 3, 604–611, Mar. 2011.
11. Wu, Y., Y. Liu, S. Li, and C. Yu, "A new wide-stopband low-pass filter with generalized coupled-line circuit and analytical theory," *Progress In Electromagnetics Research*, Vol. 116, 553–567, 2011.
12. Ma, K., J.-G. Ma, M. A. Do, and K. S. Yeo, "Characterizing and modeling conductor-backed CPW periodic band stop filter with miniaturized size," *IEEE MTT-S Int. Microwave Symp. Dig.*, 983–986, 2007.